Optimal design of a flexure hinge-based *XYZ* atomic force microscopy scanner for minimizing Abbe errors

Dongmin Kim,[a] Dongwoo Kang, Jongyeop Shim, Incheon Song, and Daegab Gweon
Department of Mechanical Engineering, KAIST (Korea Advanced Institute of Science and Technology), 373-1 Guseong-dong, Yuseong-gu, Daejeon 305-701, Republic of Korea

(Received 17 December 2004; accepted 11 April 2005; published online 29 June 2005)

To establish of standard technique of nanolength measurement in a two-dimensional plane, a new (AFM) system has been designed. In this system, measurement uncertainty is dominantly affected by the Abbe error of the *XYZ* scanning stage. No linear stage is perfectly straight; in other words, every scanning stage is subject to tilting, pitch, and yaw motion. In this article, an AFM system with minimum offset of *XYZ* sensing is designed. And, the *XYZ* scanning stage is designed to minimize the rotation angle because Abbe errors occur through the multiply of offset and rotation angle. For *XY* stage, optimal design is performed to minimize the rotation angle by maximizing the stiffness ratio of motion direction to the parasitic motion direction of each stage. For the *Z* stage, the optimal design of maximizing the first-resonant frequency is performed. When the resonant frequency increases, the scan speed is improved, thereby reducing errors caused by sensor drift. This article describes the procedures of selecting parameters for the optimal design. The full range of the *XYZ* scanner is 100 μm $\times$ 100 μm $\times$ 10 μm. Based on the solution of the optimization problem, the *XYZ* scanner is fabricated. And tilting, pitch, and yaw motion are measured by autocollimator to evaluate the performance of *XY* stage. © *2005 American Institute of Physics.* [DOI: 10.1063/1.1978827]

I. INTRODUCTION

Atomic force microscopes (AFMs) provide high-resolution, three-dimensional (3D) data and are, therefore, very useful for measuring micro- and nanostructured objects. However, as these microscopes are increasingly used for industrial applications, the requirement has been extended from high resolution to high accuracy.[1,2]

Some national standard institutes have developed a standard technique of nanolength measurement in the 3D plane,[1,3–5] but those systems have been affected by the Abbe errors of the *XYZ* scanning stage. Abbe errors occur because linear stages are not perfectly straight and every scanning stage is subject to tilting, pitch, and yaw motion. (When the motion direction is assumed as the *x* direction, roll, pitch, and yaw motion mean the rotation about and *x*, *y*, and *z* direction each.) When the measurement range increases, the uncertainty caused by Abbe errors increases. For large scanning range systems, then, Abbe errors are particularly problematic.[4,5] Additionally, it is impossible for a sensing system to have a zero offset. So, previous researchers have made attempts to reduce Abbe errors by designing AFM systems with no measuring offset (but in real systems, Abbe offsets are still present),[1,3–6] and employing control software using regression functions to compensate.[6]

In this article, we propose a new method to reduce Abbe errors by minimizing the rotation angle of the stage when lead zirconate titanate (PZT) actuator is extended. As far as the authors know, this is the first attempt to reduce Abbe errors by employing an optimal design minimizing parasitic rotation motion. Additionally, the guide mechanism has been used for same reason.

By designing a scanning stage that allows for very few Abbe errors, we can design a new instrument that is not only capable of producing topographic images of specimens with subnanometer resolution, but is also able to function as a measuring instrument with similar accuracy.

II. STRUCTURE OF THE TOTAL ATOMIC FORCE MICROSCOPY SYSTEM

A three-axis heterodyne interferometer, which is commercial product of Zygo (ZMI 2000), measures the *XYZ* dis-

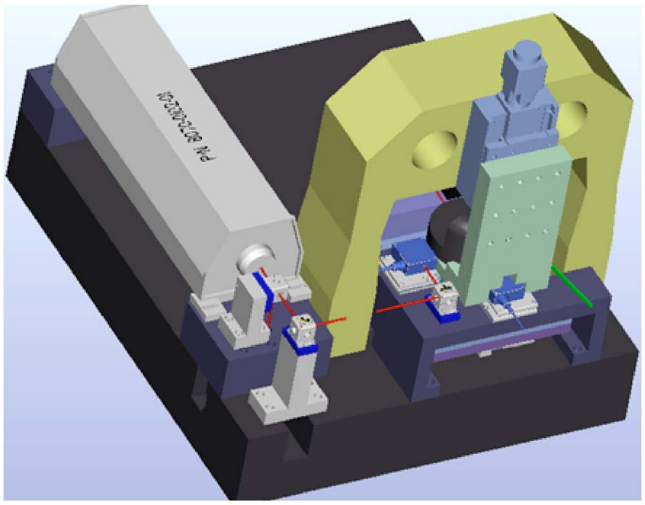

FIG. 1. Total system configuration.

[a]Electronic mail : panty78@kaist.ac.kr

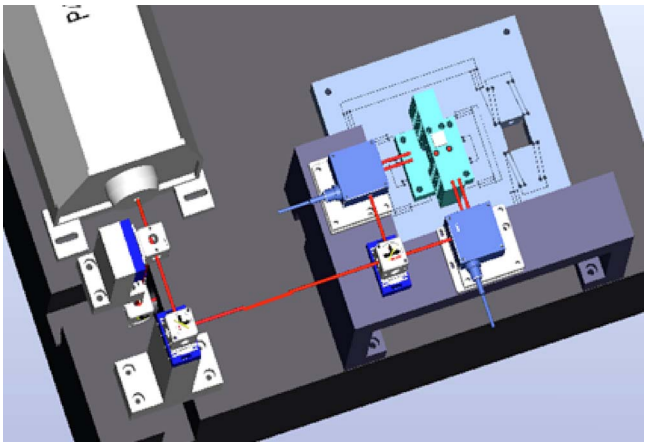

FIG. 2. *XYZ* sensing system with nearly zero Abbe offset.

placement. Each *XYZ* beam enters at the same place with the AFM tip. For a direct *Z*-axis measurement, a 90° deflection mirror placed below the sample is used to deflect the laser beam. The total system consists of a stone base, *XYZ* fine scanner, *XY* coarse stage, *Z* coarse stage, measuring head (laser source, a position sensitive photo detector (PSPD), and cantilever), *XYZ* sensing system (laser interferometer), and frame. Because high stiffness and high first-natural frequency of the system components are crucial for low noise by disturbance rejection, a cross roller guide in the *XY* coarse stage, a ball screw with harmonic drive in *Z* coarse stage, a high first natural frequency frame, and a stone base are selected. Figure 1 shows the configuration of the total system while Fig. 2 shows an *XYZ* sensing system that is designed to have no Abbe offset. *Z* optical components (a cube corner, a 90° deflection mirror, and *Z*-direction interferometer) are located inside the stone base.

III. STRUCTURE OF THE *XYZ* FLEXURE STAGE

The *XY* stage (Fig. 3) consists of two PZT actuators and

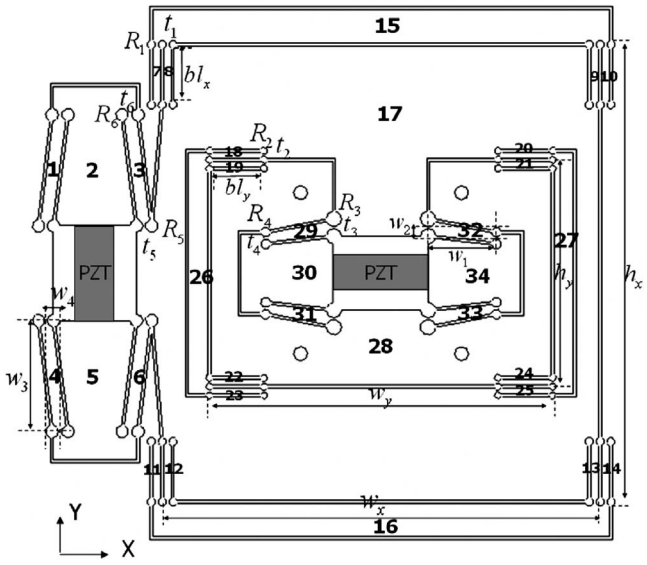

FIG. 3. Design variables and moving body number of *XY* scanner.

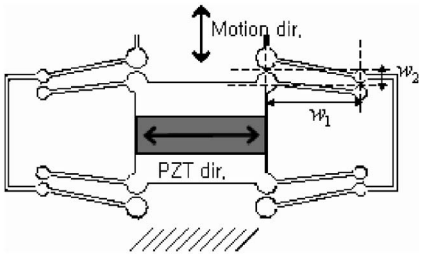

FIG. 4. Proposed motion amplification.

a monolithic flexure hinge mechanism. Each *X* and *Y* stage consists of an amplifying mechanism of motion and a guide mechanism of motion. The *Y* stage has the same structure except that it is inside the *X* stage.

A PZT actuator with a 25 μm stroke should be amplified to satisfy the maximum range of 100 μm by 100 μm. The motion amplification ratio is ω_1/ω_2. *X* and *Y* motion is decoupled. The double compound linear motion guide makes the motion straight. As a result, the *XY* stage of the single module parallel-kinematic flexure stage is made to have high orthogonality. The motion amplification mechanism that is proposed in this system has some merit. First, its symmetric structure makes the stage robust to heat. Second, this mechanism straightens the motion more than the conventional motion amplification mechanism—the lever—can. Figure 4 shows that unlike the lever mechanism shown in Fig. 5, the proposed mechanism is able to make pure linear motion.

The *Z* stage (Fig. 6) consists only of a double compound linear motion guide. The *Z* stage is located on the final moving part of the *XY* stage. The rod connects the moving part of the *Z* stage and sample jig beneath which the mirror is attached. The sample jig has a three-mirror surface which is for *XYZ* sensing. As a result, the *XYZ* stage has independent motion. *Z* sensing beam passes through the hole set at the side of PZT of the *Z* stage. As a result, there is nearly a zero-measuring offset in the *XYZ* sensing system as it is seen in Fig. 2.

Figure 7 will be helpful to understand the relation between the Abbe offset and Abbe errors more clearly. Abbe offset means the distance between the tip measuring position and each *XYZ* measuring sensor. All parasitic motions (θ_x, θ_y, and θ_z direction motions) effect the Abbe errors.

IV. MODELING OF THE STAGE MOTION

It is assumed that each hinge with a translational/rotational spring is connected with a rigid body. The spring rates of the hinge have been calculated by Paros and Weisbord equations for a single-axis flexure hinge.[7]

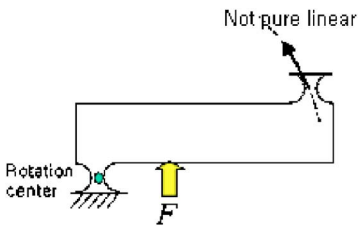

FIG. 5. Conventional motion amplification (lever).

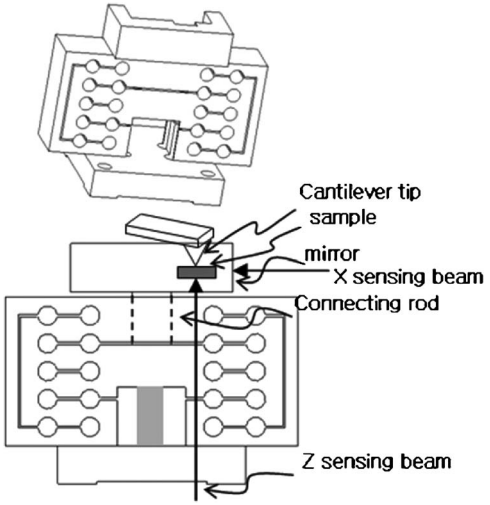

FIG. 6. The configuration of Z scanner.

From Lagrange's equation, the motion of the $XY\theta$ fine motion scanning stage can be represented by

$$Mx + Kx = F, \tag{1}$$

where M, K, and F are the system mass matrix, stiffness matrix, and force vector, respectively. The modeling method is based on Ryu's method.[8]

The system displacement vector x is defined by

$$x = [q^{1T}, \cdots, q^{iT}, \cdots, q^{N_bT}]^T, \tag{2}$$

where N_b is the number of moving bodies in the system and q_i is the displacement vector of the origin of the body i or $q_i = [x^i, y^i, z^i, \theta_x^i, \theta_y^i, \theta_z^i]^T$

In this study, we were interested in the stiffness of all six axes. Note that the size of the displacement vector x is $(6 \times 34) \times 1$ because there are 34 rigid bodies in the system, and each body has six degrees of freedom. The force vector F also has the same size, $(6 \times 34) \times 1$, and the mass matrix M and the stiffness matrix K have the same size, $(6 \times 34) \times (6 \times 34)$. The natural frequency of the system can be calculated from the given information of mass and stiffness of the system. Consider the following eigenvalue equation:

$$|K - \omega^2 M| = 0. \tag{3}$$

Note that the positive square root of the solutions of Eq. (3) are the natural frequencies of the system. The stiffness of the system can be obtained from the displacement caused by the external load at the center of the final moving body (body 28 in Fig. 3).

V. OPTIMAL DESIGN OF THE STAGE

A. *XY* stage

Optimal design based on mathematical modeling, as in the described method, is performed to obtain the best performance. Before modeling, we first simplified the model on the basis of the finite element method (FEM) simulation to make it more practical by reducing design variables using I-DEAS (commercial program). For example, the ratio between the width and length of the intermittent bar (bodies 15, 16, 26, and 27) is determined by FEM simulation to have little influence on stage stiffness. The minimum thickness of each bar, which is assumed to be a rigid body, is likewise determined. In other words, if the bar is thin, the rigid body assumption is incorrect, resulting in incorrect stiffness results. Figure 3 shows the design variables which are: Hinge thickness, hinge radii, distance between hinges, and geometric data. There are 26 design variables.

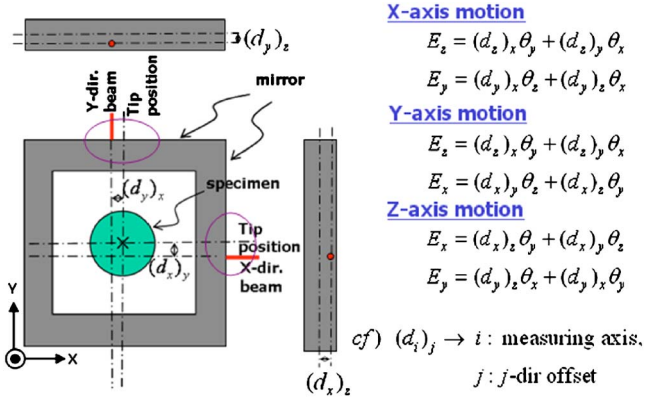

FIG. 7. The relation between sensors' offsets and their Abbe offset errors.

The objective of optimization is to minimize f (cost function), the ratio of stiffness of motion direction to that of parasitic direction. When the X and Y stages are considered with the same scale factor, the mathematical expression is as follows:

$$f = \left(\frac{k_x}{k_{\theta x} + \alpha_1 k_{\theta y} + \beta_1 k_{\theta z}} \right)_{x \text{ stage}} + \left(\frac{k_y}{k_{\theta x} + \alpha_2 k_{\theta y} + \beta_2 k_{\theta z}} \right)_{y \text{ stage}}, \tag{4}$$

where $\alpha_1, \beta_1, \alpha_2, \beta_2$ is the scale factor between rotation stiffness.

As mentioned before, all parasitic motion effects Abbe errors. Therefore, all of them should be minimized. So, the scale factor of the X and Y stages is set to be same. And also, the factor of sensitivity of $k_{\theta x}, k_{\theta y}, k_{\theta z}$ are set to be same. The stiffness of the X stage is calculated from the displacement caused by the external load at body 17. And that of Y stage can be calculated also from the displacement caused by the external load at body 28.

This optimal problem includes many constraints. For example, the maximum stress at the hinge point should be less

TABLE I. Constants used for XY stage design.

Constant	α_1	α_2	α_3	α_4	α_5	α_6	C_1	C_2	h_{inner}	h_{outer}	l_{pzt}
Values	1/15	1/8	1/8	1/15	$h_{\text{inner}}/4$	1/8	150	160	20	20	27

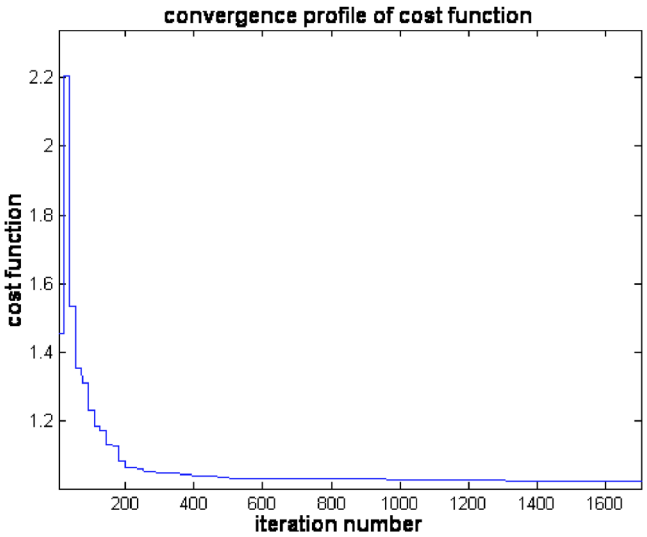

FIG. 8. Convergence profile of cost function.

than the yield stress. There are also constraints for the system size, motion range, natural frequency, and beam assumption.

First, consider the maximum stress constraints. The maximum stress occurs at the hinge point with the minimum thickness. Maximum stress is calculated by Eq. (5)

$$\sigma_{\max} = \frac{6M_z K_t}{t^2 b}, \tag{5}$$

where t is the hinge thickness, b is the hinge width, M_z is the moment at the hinge, and K_t is a stress concentration factor. Let k_z be the rotational stiffness of the hinge, then

$$M_z = k_z \theta. \tag{6}$$

Because the maximum rotational movement occurs when each piezoelectric actuator reaches its maximum elongation, the maximum allowable rotation at the hinge is

$$g_j = S_f \theta_z^j - \frac{t_i^2 b}{6 k_z^i K_t} \sigma_Y < 0, \tag{7}$$

where $j=1,\ldots,6$, S_f is a safety factor, and σ_Y is the yield stress of the hinge material. There are six constraints for stress. As in Fig. 3, let θ_z^j be the rotational movement of body i with respect to the Z axis, k_z^i be the rotational stiffness of hinge i, and t_i be the minimum thickness of hinge i.

Second, consider the constraints for the system size. There are some constants, shown in Table I. α_i is obtained from FEM and is determined to have little influence on stage stiffness. C_i is related to the size of the stage.

$$g_7 = 2bl_x + 8R_1 - h_x < 0,$$

$$g_8 = h_x + 2\alpha_1 w_x - C_1 < 0,$$

$$g_9 = w_x + 2w_4 + h_{\text{outer}} + t_5 + 3R_5 - C_2 < 0,$$

$$g_{10} = 2(t_1 + 2R_1) + 2R_1 - w_x < 0,$$

$$g_{11} = h_{\text{inner}} + 2w_2 + t_3 + 2R_3 + 2\alpha_2(w_y - 2bl_y - 8R_2) - [h_y - 2(t_2 + 2R_2)] < 0,$$

TABLE II. The starting points of design variables and optimal results.

	Design variables sets					
	Start points				Optimum and design values	
Design variables (mm)	1	2	3	4	S_{opt}	S_{design}
R_1	1	5	2	4	1.2182	1.2
R_2	5	8	1	6	1.0000	1.0
R_3	2	3	5	9	2.1983	2.2
R_4	10	5	2	7	1.4387	1.4
R_5	8	2	3	5	1.7769	1.8
R_6	7	4	3	6	1.8119	1.8
t_1	2	1	2	3	0.7206	0.7
t_2	1	3	1	1	0.5000	0.5
t_3	3	2	2	1	0.5000	0.5
t_4	2	3	2	1	0.5000	0.5
t_5	1	1	3	2	0.7387	0.7
t_6	2	1	1	2	0.9144	0.9
bl_x	3	8	15	25	14.6676	14.7
bl_y	5	25	10	15	13.5698	13.6
w_x	100	120	140	130	125.2155	125.2
h_x	130	120	100	150	132.7813	132.8
w_y	100	90	120	80	100.2474	100.2
h_y	90	110	100	80	64.6568	64.7
w_1	3	20	40	60	19.5296	19.5
w_2	10	60	3	20	3.0197	3.0
w_3	60	15	20	30	31.7291	31.7
w_4	20	3	60	20	3.9877	4.0

TABLE III. The six-axis stiffness of S_{opt} and S_{design} (XY stage).

	S_{opt}	S_{design}
k_x	0.664(N/μm)	0.621(N/μm)
k_y	0.365(N/μm)	0.364(N/μm)
k_z	49.4(N/μm)	49.1(N/μm)
$k_{\theta x}$	78.6(Nm/mrad)	78.4(Nm/mrad)
$k_{\theta y}$	127(Nm/mrad)	126(Nm/mrad)
$k_{\theta z}$	445(Nm/mrad)	445(Nm/mrad)

TABLE IV. The six-axis stiffness of S_{design} (Z stage).

	S_{design}
k_x	2098(N/μm)
k_y	470(N/μm)
k_z	47(N/μm)
$k_{\theta x}$	81.9(Nm/mrad)
$k_{\theta y}$	374.6(Nm/mrad)
$k_{\theta z}$	255.3(Nm/mrad)

$$g_{12} = 2bl_y + 8R_2 - w_y < 0,$$

$$g_{13} = 2(t_2 + 2R_2) + 2R_2 - h_y < 0,$$

$$g_{14} = h_y + 2(t_2 + 2R_2) + 2\alpha_3[w_x - 2(t_1 + 2R_1) - 2R_1] - (h_x - 2bl_x - 8R_1) < 0,$$

$$g_{15} = w_y + 2\alpha_4 h_y + 2\alpha_4(h_x - 2bl_x - 8R_1) - w_x < 0,$$

$$g_{16} = l_{PZT} + 2(R_3 + R_4) + 2w_1 + 2\alpha_5 + 2\alpha_6[h_y - 2(t_2 + 2R_2)] + 2R_2 - w_y < 0,$$

$$g_{17} = l_{PZT} + 2w_3 + 2R_6 + 2\alpha_2 h_{outer} - h_x < 0.$$

Third, consider the constraint for the full range of the XY scanner. The maximum range of the X scanner (X_{max}) is obtained by calculating the force that is added in bodies 2 and 5. The force is determined by the ratio of the stiffness of PZT and that of between bodies 2 and 5. Using the same method, the maximum range of the Y scanner (Y_{max}) is obtained. Their constraint is as follows.

$$g_{18} = X_{designed} - X_{max} < 0,$$

$$g_{19} = Y_{designed} - Y_{max} < 0,$$

where $X_{designed}$ and $Y_{designed}$ are 120 μm each and the safety factor is 20%.

Fourth, consider the first-natural frequency. The first-natural frequency f_n can be obtained from Eq. (3) and must satisfy the following constraint:

$$g_{20} = 100 - f_n < 0.$$

The XY scanner is designed to have a natural frequency of more than 100 Hz.

Fifth, assuming that the connecting body (7–14 and 18–25) is rigid, the stiffness of the body is restricted by 15 times higher than the stiffness of the final moving part. That is also why the stiffness of body does not influence to stage stiffness. So, for bodies 7–14 and 18–25, their stiffness of X direction, $k_{x\_beam\_x}$ is $4(3EI_x^x/bl_x^3)$ where E is Young's modulus, $I_x^x = b(t_1+2R_1)^3/12$. Their stiffness of Z direction, $k_{x\_beam\_z}$ is $4(3EI_x^z/bl_x^3)$, $I_x^z = b^3(t_1+2R_1)/12$, which is the same for bodies 18–25.

$$g_{21} = 15k_{final}^x - k_{x\_beam\_x} < 0,$$

$$g_{22} = 15k_{final}^z - k_{x\_beam\_z} < 0,$$

$$g_{23} = 15k_{final}^y - k_{y\_beam\_y} < 0,$$

$$g_{24} = 15k_{final}^z - k_{y\_beam\_z} < 0.$$

B. *Z* stage

For Z stage, the optimal design of maximizing first-resonant frequency is performed. Similar to the XY stage constraints, the constraints for the Z stage are for maximum stress (which is less than yield stress), stage size (which enables locate on Y stage), motion range (which is 12 μm with a 20% safety factor), and beam assumption constraints. If resonant frequency increases, scan speed is improved, thereby reducing errors caused by sensor drift. Additionally, the motion range of the Z stage is smaller than the XY stage.

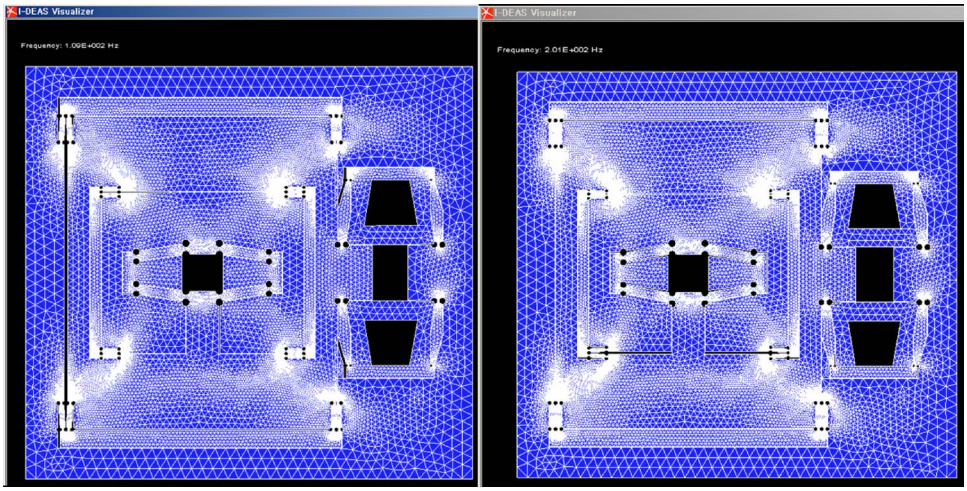

FIG. 9. FEM simulation of XY scanner.

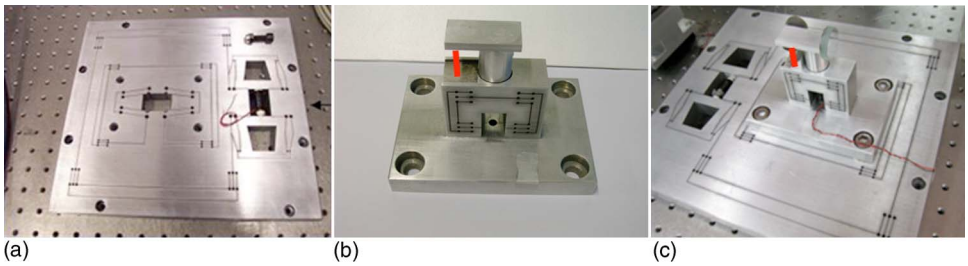

FIG. 10. The picture of *XYZ* stage: (a) *XY* stage, (b) *Z* stage, and (c) *XYZ* stage.

So the induced parasitic directional rotations are less, thereby Abbe errors being far fewer than in the *XY* stage. Generally, the most critical performance value of the *Z* stage is first-natural frequency, so it is selected as a cost function. The detailed procedure is omitted because it duplicates the XY optimal design procedure.

VI. DESIGN RESULTS

For the optimal design a sequential quadratic programming method and MATLAB were used. This method does not always guarantee the global minimum. Therefore, in this study, four different starting points have been used to verify the global minimum and the same minimum values have been provided, regardless of the starting points. The convergence profile of cost function is shown in Fig. 8. The obtained optimum design parameters are given in Table II. It may be noted that for manufacturing reasons, the parameter value used in the actual design is not exactly the same as the theoretical optimum values.

When using S_{design}, cost function is 1.02×10^{-2}. The optimal cost function value is 0.96×10^{-2}, so the design value and optimal value have a difference of 6%. In Table III, the six-axis stiffness of both S_{opt} and S_{design} are shown.

The design results are as follows. The natural frequency of the *X* and *Y* stages is 127 Hz and 220 Hz, respectively, and FEM results are 133 Hz and 225 Hz, resulting in a difference of 4.5% and 2.2% each. The full range is 120.8 μm for *X* and 130 μm for *Y*, and FEM results are 110 μm and 123.6 μm, resulting in a difference of 8.9% and 4.9% each. The FEM result verifies that the modeling is reasonable. Figure 9 shows FEM simulation.

For the *Z* stage, the resonant frequency is 2.86 kHz and its six-axis stiffness is represented in Table IV. And it has the 11 um full motion range.

With these optimal results, the *XYZ* flexure stage is fabricated (Fig. 10) out of a single piece of 20 mm thick, hardened aluminum alloy, containing 4.7% Zn, 3.1% Mg, and 0.6% Cu (AL 7075).

VII. EXPERIMENT AND RESULTS

To check the effect of this design method, the generated rotational motions are measured using autocollimator which has 0.05 arcs resolution. Maximum rotational motion is 0.75 arcs in the direction of yaw motion about the full range motion 100 μm by 100 μm in the *X*, *Y* direction. Experimental results are shown in Fig. 11. From these results, when we suppose Abbe's offset is 0.5 mm, the Abbe's error will be within 1.82 nm.

Generally, it is so difficult to make the stage have below a 1 arcs parasitic motion about rotational direction (pitch, yaw, and roll motion). So, we think this optimal design had an effect on reducing parasitic rotational motion.

VIII. DISCUSSION

To establish a standard technique for nanolength measurement in a two-dimensional (2D) plane, a new AFM system is designed that has no offset of *XYZ* sensing, and a new AFM scanning stage is proposed. Additionally, the *XYZ* decoupled scanning stage is designed to have a minimum of Abbe errors for the *XY* stage and a high scanning speed for the *Z* stage. This article has presented the optimal design procedure for this system in which the *XYZ* scanning stage has the full range of 110 $\mu m\times123.6$ $\mu m\times11$ μm. By FEM simulation, the full range and first-natural frequency are verified. Based on the solution of the optimization problem, the *XYZ* scanner is fabricated.

The proposed stage has 0.75, 0.70 arcs error about 100 μm by 100 μm motion range in the *X* and *Y* directions.

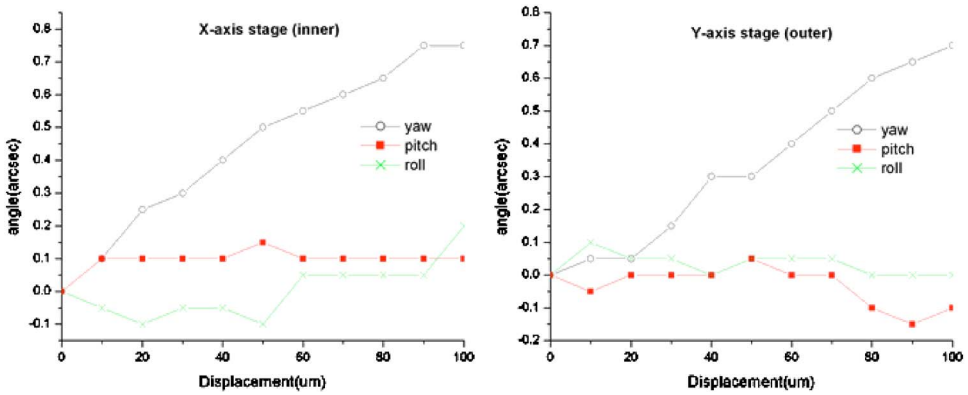

FIG. 11. Rotation angle of *XY* scanner about full range motion.

When the Abbe offset is supposed as 0.5 mm, the Abbe's error can be 1.82 nm. This quantity is very small compared with other standard institutes. Soon, the total AFM system will be completed. Then, we will obtain total measurement uncertainty.

ACKNOWLEDGMENT

The authors would like to thank the MOCIE (Ministry of Commerce, Industry and Energy of Korea) for its funding of this work.

[1] M. Bienias, S. Gao, K. Hasche, R. Seeman, and K. Thiele, Surf. Interface Anal. **25**, 606 (1997).
[2] J. Garnaes, N. Kofod, A. Kuhle, C. Nielsen, K. Dirscherl, and L. Blunt, Precis. Eng. **27**, 91 (2003).
[3] R. G. Dixon, Proc. SPIE **3677**, 20 (1999).
[4] F. Meli and R Thalmann, Meas. Sci. Technol. **9**, 1087 (1998).
[5] S. Gonda, T. Doi, T. Kurosawa, and Y. Tanimura, Rev. Sci. Instrum. **70**, 3362 (1999).
[6] K. Hasche, K. Herrmann, W. Mirande, R. Seemann, L. Vitushkin, M. Xu, and G. Yu, Surf. Interface Anal. **33**, 71 (2002).
[7] J. M. Paros and L. Weisbord, Mach. Des. **37**, 151 (1965).
[8] J. W. Ryu, Precis. Eng. **21**, 18 (1997).